A three-dimensional imaging technique for a directional borehole radar

Koen W.A. van Dongen*, Peter M. van den Berg‡ and Jacob T. Fokkema‡

* T&A RADAR,
Badhuisweg 3, PO Box 37060, 1030 AB Amsterdam, The Netherlands
‡ Centre for Technical Geoscience, Delft University of Technology,
PO Box 5031, 2600 GA Delft, The Netherlands

ABSTRACT

In this paper we describe a directional borehole radar system. We first present the simulation and design of the antenna system. The antennas are positioned in a bistatic setup. In order to obtain a focused radiation pattern the transmitting and receiving dipoles are each shielded with a curved reflector. The radiation pattern of this scattered wavefield is computed by solving the integral equation for the unknown electric surface current at the conducting surface. Based on these numerical simulations, a prototype has been built. The radiation pattern measured in the plane perpendicular to the antenna is in good agreement with the computed pattern. Subsequently, we discuss a three-dimensional imaging method for this borehole radar. The computed radiation pattern is used in such a way that deconvolution for the angular radiation pattern can be applied. Some preliminary imaging results will be presented.

Keywords: ground penetrating radar, directional borehole radar, 3D imaging, inversion, deconvolution, electromagnetic waves

1. INTRODUCTION

In the geophysical characterization of the shallow subsurface there is a great demand for directional borehole radar systems. To meet this demand, we have developed a radar system which has enough resolution and penetrating power, fits in a single borehole and has a directional radiation pattern. In this paper we present the simulation and design of the antenna system for a borehole radar. The antennas are positioned in a bistatic setup. In order to obtain a focused radiation pattern the transmitting and receiving dipoles are each shielded with a reflector. The transient generated wavefield, with a centre frequency of 100 MHz, is reflected in the desired direction by a perfectly conducting cylindrically curved plate. The radiation pattern of this scattered wavefield is computed by solving the integral equation for the unknown electric surface current at the conducting surface. The method is based on the conjugate gradient FFT solution as developed by Zwamborn and Van den Berg.[1] Once the electric current distributions at the dipole and the reflector are known, the radiated wavefield can be determined using an integral representation over the wire and the curved plate. A prototype has been built and the simulated data are compared with experimental results. The radiation pattern measured in the plane perpendicular to the antenna is in good agreement with the computed one. Subsequently, we discuss a three-dimensional imaging method for this borehole radar. We employ a linearization of the inversion problem using the Born approximation. In first instance we apply a back-propagation algorithm using the synthetic radiation patterns of the antenna system. To improve the imaging, we use the back-propagation results in a minimization procedure. A full (linear) inversion method based on the conjugate gradient minimization is proposed in such a way that a deconvolution for the angular radiation pattern is achieved. Based on synthetic data with noise some imaging results of the different approaches are presented.

2. ANTENNA SYSTEM

The antenna system consists of an electric dipole which is partly shielded by a reflector, see figure 1(a). The aim is to compute the radiation pattern of the complete antenna system. Therefore an integral equation is derived, which relates the known incident electric wavefield from the electric dipole antenna to the unknown electric current density at the surface of the reflector. Subsequently this integral equation is solved via FFT Conjugate Gradient method[1] and finally the total field is computed. Furthermore, a numerical example will be shown and some of the numerical results are verified with experimental results.

Send correspondence to Koen van Dongen, email: vandongen@ta-radar.nl .
published in: *SPIE's 46th Annual Meeting, Subsurface and Surface Sensing Technologies and Applications III, July 30 - August 1, 2001, San Diego CA, USA, Vol. 4491, pp. 88-98.*

2.1. Antenna Configuration

The antenna system consists of an electric dipole antenna and a reflector. The spatial domain $\mathbb{D}$ of the dipole is defined in a Cartesian coordinate system as

$$\mathbb{D} = \{x_k \in \mathbb{R}^3 | -x^d < x < x^d, y = y^d, z = z^d\} \ . \tag{1}$$

Next to the dipole, a rectangular circular cylindrically curved perfectly conducting plate, the reflector, is positioned, see figure 1(a). Since the curvature of the reflector is cylindrical, an orthogonal circular cylindrical coordinate system is introduced, see figure 1(b). The correspondence between a position vector $\underline{x} = x_i = (x, y, z)$ in the Cartesian coordinate system and a position vector $\underline{v} = v_i = (x, r, \phi)$ in the circular cylindrical system is given by

$$x = x \ , \qquad y = r\cos(\phi) \ , \qquad z = r\cos(\phi) \ . \tag{2}$$

Furthermore, a coordinate transformation matrix T_{ij} is defined via

$$u_{x_i} = \mathsf{T}_{ij} u_{v_j} \ , \tag{3}$$

and the inverse T_{ij}^{-1} for the transformation from the cylindrical to the Cartesian coordinate system. We define the quantity $Q_{v_i}(\underline{x})$ to be in a cylindrical coordinate system with a position specified by the vector $\underline{x}$ in the Cartesian coordinate system. Finally, the area $\mathbb{A}$ of the reflector in a cylindrical coordinate system is defined as

$$\mathbb{A} = \{v_k \in \mathbb{R}^3 | -x^a < x < x^a, r = r^a, -\phi^a < \phi < \phi^a\} \ , \tag{4}$$

see figure 1.

The background medium in which the antenna configuration is embedded is a homogeneous medium that is, in addition, linear, time-invariant, instantaneously reacting, locally reacting and isotropic in its electromagnetic behaviour, with permittivity ε, permeability μ_0 and conductivity σ. Here ε equals

$$\varepsilon = \varepsilon_0 \varepsilon_r \ , \tag{5}$$

with ε_0 the permittivity of vacuum and with ε_r the relative permittivity of the medium.

All computations are carried out in the temporal Laplace domain with Laplace parameter $s = -i\omega$, where ω equals $2\pi f$ with f the frequency. Therefore the symbol '$\hat{}$' is used to indicate that the specified quantity is in this temporal Laplace domain, e.g. $\hat{Q} \equiv Q(\omega)$.

2.2. Formulation of Integral Equation

The total electric wavefield, $\hat{E}^{\text{tot}}_{x_i}(x_m)$, is a summation of the incident electric wavefield from an electric dipole, $\hat{E}^{\text{inc}}_{x_i}(x_m)$, and the wavefield scattered on the reflector, $\hat{E}^{\text{sct}}_{x_i}(x_m)$,

$$\hat{E}^{\text{tot}}_{x_i}(v_m) = \hat{E}^{\text{inc}}_{x_i}(v_m) + \hat{E}^{\text{sct}}_{x_i}(v_m) \ , \quad \forall \ v_m \in \mathbb{R}^3 \ . \tag{6}$$

From Maxwell equations it can be derived that the incident wavefield in a cylindrical coordinate system equals

$$\hat{E}^{\text{inc}}_{v_i}(v_m) = \left(-\gamma^2 \delta_{ij} + \nabla_{v_i}\nabla_{v_j}\cdot\right) \mathsf{T}_{jl} \frac{1}{s\varepsilon} \int_{v'_m \in \mathbb{D}} \hat{G}(v_m|v'_m) \mathsf{T}_{lm} \hat{J}^{\text{dip}}_{v_m}(v'_m) \text{dL}(v'_m) \ , \tag{7}$$

with

$$\gamma^2 = s^2(\varepsilon + \frac{\sigma}{s})\mu_0 \ , \tag{8}$$

δ_{ij} the Kronecker delta tensor, $\nabla_{v_i}\nabla_{v_j}\cdot$ the gradient divergence operator, $\hat{G}(v_m|v'_m)$ the Green function of the background medium, $\hat{J}^{\text{dip}}_{v_j}(v'_m)$ the electric surface current density at the dipole.

The scattered wavefield is caused by an electric surface current density at the surface of the reflector, due to the presence of the incident electric wavefield. At this surface, electromagnetic boundary conditions require that

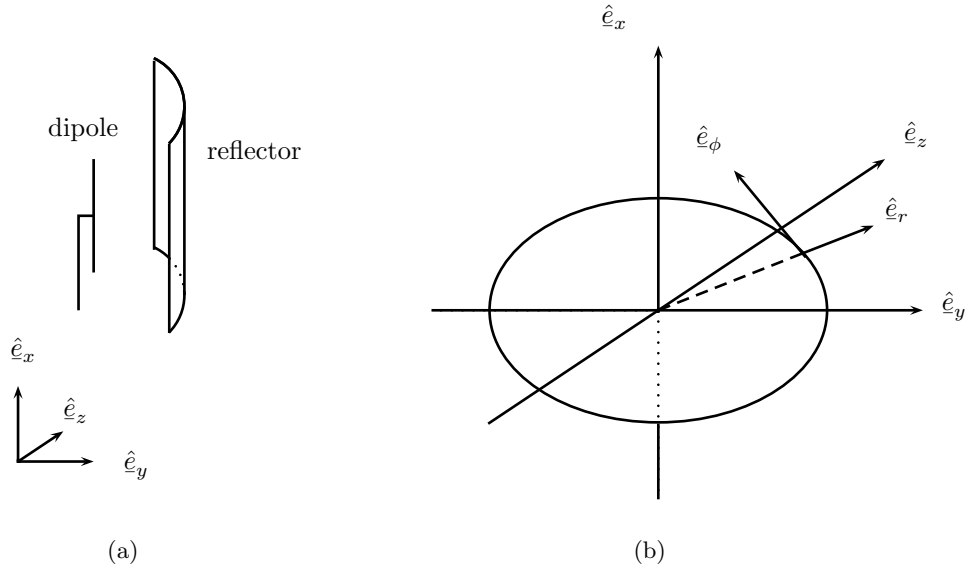

(a) (b)

Figure 1. The antenna configuration (a) and the two coordinate systems (b), the Cartesian with unit vectors $(\hat{\underline{e}}_x, \hat{\underline{e}}_y, \hat{\underline{e}}_z)$ and the cylindrical with unit vectors $(\hat{\underline{e}}_x, \hat{\underline{e}}_r, \hat{\underline{e}}_\phi)$.

components of the total electric field, $\hat{E}^{\text{tot}}_{v_i}(v_m)$, tangential to this surface vanish. In a cylindrical coordinate this results in the following equation

$$\hat{E}^{\text{sct}}_{v_\alpha}(v_m) = -\hat{E}^{\text{inc}}_{v_\alpha}(v_m) \ , \quad \forall \ v_m \in \mathbb{A} \ , \quad \forall \ \alpha \in \{1,3\} \ , \tag{9}$$

where $\hat{E}^{\text{sct}}_{v_\alpha}(v_m)$ is the wavefield scattered on the reflector. Note that we introduced quantities with Greek subscripts (α) to denote the two tangential components of the field quantities. Consequently, the following integral equation is obtained

$$-\hat{E}^{\text{inc}}_{v_\alpha}(v_m) = \left(-\gamma^2\delta_{\alpha j} + \nabla_{v_\alpha}\nabla_{v_j}\cdot\right) \mathsf{T}_{jl} \frac{1}{s\varepsilon} \int_{v'_m \in \mathbb{A}} \hat{G}(v_m|v'_m)\mathsf{T}_{l\beta}\hat{J}^{\text{rfl}}_{v_\beta}(v'_m)\text{dA}(v'_m) \ , \quad \forall \ v_m \in \mathbb{A} \ . \tag{10}$$

Note that there are two unknown quantities, the two components of the electric surface current density at the reflector, $\hat{J}^{\text{rfl}}_{v_\beta}(v'_m) = \left(\hat{J}^{\text{rfl}}_x(v'_m), 0, \hat{J}^{\text{rfl}}_\phi(v'_m)\right)$, and two known quantities, the two components of the incident electric field at the reflector, $\hat{E}^{\text{inc}}_\beta(v_m) = \left(\hat{E}^{\text{inc}}_x(v_m), 0, \hat{E}^{\text{inc}}_\phi(v_m)\right)$. To solve this integral equation via the FFT Conjugate Gradient method, an operator notation and a definition of a norm is required. Using the operator notation, equation (10) is formulated as

$$\mathsf{f}_{v_\alpha} = (\mathsf{Lj})_{v_\alpha} \ , \tag{11}$$

where f_{v_α} describes the known incident wavefield, and $(\mathsf{Lj})_{v_\alpha}$ describes the differential/integral operation of the right-hand side of equation (10). Furthermore, the norm is defined via the inner product of two vectorial quantities in the spatial domain $\mathbb{A}$, viz.

$$\|v_{v_\alpha}\|_{\mathbb{A}} = \langle v_{v_\alpha}, \overline{v}_{v_\alpha}\rangle_{\mathbb{A}} = \sum_{l,n} \left(v_{x;ln}\overline{v}_{x;ln} + v_{\phi;ln}\overline{v}_{\phi;ln}\right) r^a \Delta x \Delta\phi \ , \tag{12}$$

where the subscripts l and n refer to the position of the quantity in the discretized reflector domain with elements of size Δx and $\Delta\phi$ in the $\hat{e}_x$ and $\hat{e}_\phi$ direction. Next an error norm is defined as the difference between the known incident field, f, and the computed field based on the approximated electric surface current density, j,

$$r_{v_\alpha} = \| \left(\mathsf{Lj}\right)_{v_\alpha} - \mathsf{f}\|_{\mathbb{A}} \ . \tag{13}$$

The adjoint of the operator L, L^*, is also required and defined via the inner product as

$$\langle r_{v_\alpha}, (\mathsf{Lj})_{v_\alpha}\rangle_{\mathbb{A}} = \langle (\mathsf{L}^*\mathsf{r})_{v_\alpha}, j_{v_\alpha}\rangle_{\mathbb{A}} \ . \tag{14}$$

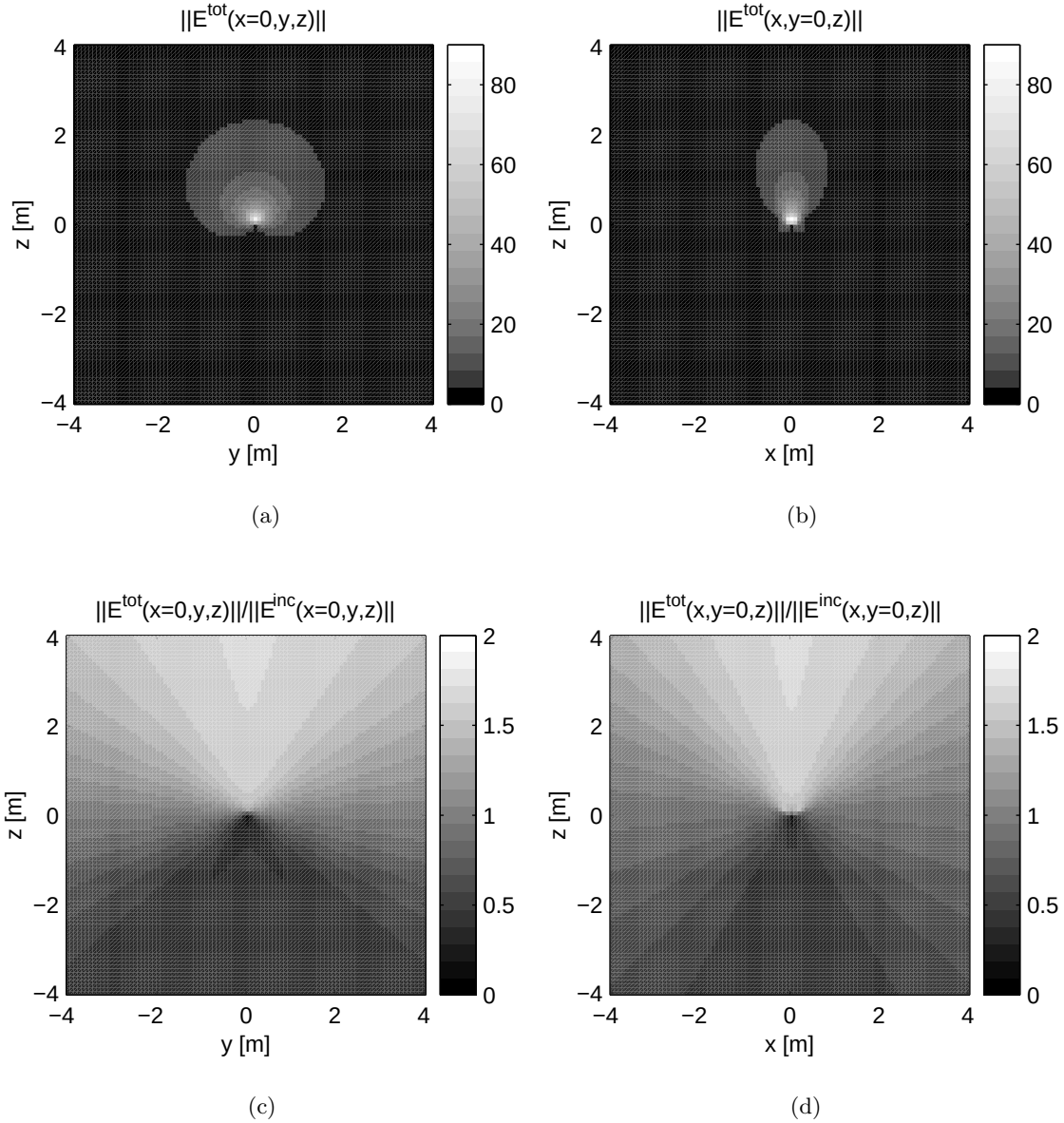

Figure 2. For a background medium which has a relative permittivity of $\varepsilon_r = 81$, a relative permeability of $\mu_r = 1$ and a conductivity $\sigma = 0$ S/m (a) (b) the total electric wavefield, $\|E^{\mathrm{tot}}\|$, and (c) (d) the total electric wavefield normalized by the incident wavefield $\|E^{\mathrm{inc}}\|$.

Finally, the normalized error function ERR, which is minimized, is defined as

$$\mathrm{ERR} = \frac{\|r_{v_\alpha}\|_{\mathbb{A}}}{\|\hat{E}^{\mathrm{inc}}_{v_\alpha}\|_{\mathbb{A}}} \,. \tag{15}$$

2.3. Numerical Results and Experimental Verification of the Antenna Model

Computations are carried out to design an 'optimal' configuration. For such an optimal configuration a prototype has been built. Of this prototype the radiation pattern is measured and compared with the simulations.

In figure 2 the results of the computations are shown for the optimal configuration which fits in a single borehole of 0.10 m in diameter. The electric current through the dipole is described by a cosine shaped 100 MHz distribution,

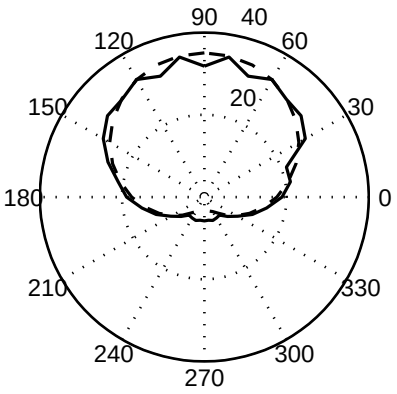

Figure 3. The measured radiation pattern, solid line, and the computed one, dashed line.

maximal in the center and zero at the both tips. The background medium has a relative permittivity of $\varepsilon_r = 81$, relative permeability of $\mu_r = 1$ and is non-conducting, $\sigma = 0$ S/m. After solving the integral equation the total electric wavefield is computed in the xz- and the yz-plane, see figures 2(a) and 2(b). To quantify the field scattered at the reflector, we define a gain factor, $\|E^{\text{tot}}\|/\|E^{\text{inc}}\|$, see figures 2(c) and 2(d).

Based on this optimal configuration a prototype has been built. The radiation pattern of this prototype is measured at a radial distance of $r = 0.3$ m in the plane $x = 0$ m. In figure 3 the measured and computed radiation pattern are shown. The difference in energy between the measured and computed radiation patterns, $\|E^{\text{comp}} - \alpha E^{\text{meas}}\|$, is minimized via α, where α equals

$$\alpha = \frac{\langle E^{\text{meas}}, E^{\text{comp}} \rangle}{\langle E^{\text{meas}}, E^{\text{meas}} \rangle} \ , \tag{16}$$

with E^{meas} and E^{comp} the measured and computed radiation patterns respectively. Note that the patterns are in excellent agreement.

3. CHANGE OF ANTENNA IMPEDANCE DUE TO SCATTERING OBJECTS

A relation describing the change of impedance due to the presence of objects in the subsurface is derived from the reciprocity theorem.[2] In figure 4 two states A and B are shown. In state A, the source free spatial domain $\mathbb{D}$ with boundary $\partial\mathbb{D}$ and normal ν_i contains a homogeneous background medium that is, in addition, linear, time-invariant, instantaneously reacting, locally reacting and isotropic in its electromagnetic behaviour. The medium is described by the parameters $\hat{\eta}(\underline{x})$,

$$\hat{\eta}(\underline{x}) = \sigma(\underline{x}) + s\varepsilon(\underline{x}) \ , \tag{17}$$

and $\hat{\zeta}(\underline{x})$,

$$\hat{\zeta}(\underline{x}) = s\mu(\underline{x}) \ , \tag{18}$$

see table 1. The domain encloses an inaccessible volume action antenna source domain $\mathbb{D}^{\text{src}} \not\subset \mathbb{D}$ containing the transmitting and receiving antennas. The only fields present are the electromagnetic background wavefields. In state B, the same domain $\mathbb{D}$ with boundary $\partial\mathbb{D}$ is described by the same medium parameters, and this time it also encloses a domain $\mathbb{D}^{\text{sct}}$, due to the presence of an object with medium parameters $\hat{\eta}^{\text{sct}}(\underline{x})$ and $\hat{\zeta}^{\text{sct}}(\underline{x})$. For these two states the reciprocity theorem is given as

$$\begin{aligned}
\epsilon_{m,r,p} \int_{x_i \in \partial\mathbb{D}} \nu_m \left[\hat{E}_r^A(\underline{x}) \hat{H}_p^B(\underline{x}) - \hat{E}_r^B(\underline{x}) \hat{H}_p^A(\underline{x}) \right] \mathrm{dA} \\
= \int_{x_i \in \mathbb{D}} \left(-[\eta^B(\underline{x}) - \eta^A(\underline{x})] \hat{E}_k^A(\underline{x}) \hat{E}_k^B(\underline{x}) + [\zeta^B(\underline{x}) - \zeta^A(\underline{x})] \hat{H}_j^A(\underline{x}) \hat{H}_j^B(\underline{x}) \right) \mathrm{dV} \\
+ \int_{x_i \in \mathbb{D}} \left(\hat{J}_k^A(\underline{x}) \hat{E}_k^B(\underline{x}) - \hat{K}_j^A(\underline{x}) \hat{H}_j^B(\underline{x}) - \hat{J}_r^B(\underline{x}) \hat{E}_r^A(\underline{x}) - \hat{K}_p^B(\underline{x}) \hat{H}_p^A(\underline{x}) \right) \mathrm{dV} \ .
\end{aligned} \tag{19}$$

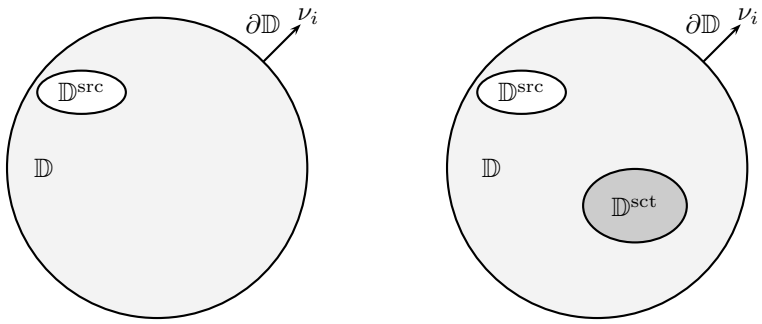

(a) (b)

Figure 4. Two states of the same spatial domain $\mathbb{D}$ and with inaccessible volume action antenna source domain $\mathbb{D}^{\text{src}} \not\subset \mathbb{D}$. The source domain contains a receiving and transmitting antenna. In state A (a) the electromagnetic properties are $\hat{\eta}^A(\underline{x}) = \hat{\eta}(\underline{x})$, $\hat{\zeta}^A = \hat{\zeta}$ and in state B (b) there is same background medium and a scattering domain $\mathbb{D}^{\text{sct}} \subset \mathbb{D}$, with $\hat{\eta}^B(\underline{x}) = \hat{\eta}^{\text{sct}}(\underline{x})$, $\hat{\zeta}^B(\underline{x}) = \hat{\zeta}(\underline{x})$.

In the left-hand side of this equation, Maxwell equations are applied to approximate $\hat{E}_i(\underline{x})$ on the source free surface of the source domain in the low frequency range by

$$\hat{E}_i(\underline{x}) = -\partial_i \hat{\phi}(\underline{x}) \ . \tag{20}$$

In combination with Stokes theorem, the integral over the inner boundary of the source domain $\partial\mathbb{D}^{\text{src}}$ is rewritten as

$$\epsilon_{m,r,p} \int_{x_i \in \partial\mathbb{D}^{\text{src}}} \nu_m \left[\hat{E}_r^A(\underline{x}) \hat{H}_p^B(\underline{x}) - \hat{E}_r^B(\underline{x}) \hat{H}_p^A(\underline{x}) \right] \mathrm{dA} = \int_{x_i \in \partial\mathbb{D}^{\text{src}}} \nu_m \left[\hat{\phi}^A(\underline{x}) \hat{\eta}^B(\underline{x}) \hat{E}_m^B(\underline{x}) - \hat{\phi}^B(\underline{x}) \hat{\eta}^A(\underline{x}) \hat{E}_m^A(\underline{x}) \right] \mathrm{dA} \ . \tag{21}$$

The antennas in the source domain are described as perfect conductors which form a N-port system, where each termination port has a surface $\mathbb{A}_\alpha$, for $\alpha = 1, \ldots, N$. Since the electric potential $\hat{\phi}(\underline{x})$ is constant over such a termination port, each terminal α has a constant potential $\hat{V}_\alpha$. At each port the Maxwell current density $\hat{J}_k(\underline{x}) + s\hat{D}_k(\underline{x})$ is dominated by the electric current density $\hat{J}_k(\underline{x})$ in the low frequency approximation and consequently the electric current I_α is used. Consequently, using the constitutive relations in combination with the electromagnetic boundary conditions the right hand side of equation (21) equals

$$\int_{x_i \in \partial\mathbb{D}^{\text{src}}} \nu_m \left[\hat{\phi}^A(\underline{x}) \hat{\eta}^B(\underline{x}) \hat{E}_m^B(\underline{x}) - \hat{\phi}^B(\underline{x}) \hat{\eta}^A(\underline{x}) \hat{E}_m^A(\underline{x}) \right] \mathrm{dA} = \sum_{\alpha=1}^{N} \int_{x_i \in \mathbb{A}_\alpha} \nu_m \left[\hat{\phi}^A(\underline{x}) \hat{J}_m^B(\underline{x}) - \hat{\phi}^B(\underline{x}) \hat{J}_m^A(\underline{x}) \right] \mathrm{dA} \tag{22}$$

$$= \sum_{\alpha=1}^{N} \left[\hat{V}_\alpha^A \hat{I}_\alpha^B - \hat{V}_\alpha^B \hat{I}_\alpha^A \right] \ . \tag{23}$$

Note that the contribution of the integral over the remaining outer boundary of the domain $\mathbb{D}$ equals zero. This can be observed by applying the far field approximation to these wavefields.

The electric potentials and line current densities in the antennas are coupled via the impedance matrix $\hat{Z}_{\alpha\beta}$ as

$$\hat{V}_\alpha = \hat{Z}_{\alpha\beta} \hat{I}_\beta \qquad \text{for } \{\alpha, \beta\} = 1, \ldots, N \ . \tag{24}$$

Combining equations (19), (23) and (24), and using the state descriptions as formulated in table 1 result in

$$\delta \hat{Z}_{\alpha\beta} \hat{I}_\alpha^A \hat{I}_\beta^B = -\int_{x_i \in \mathbb{D}} [\eta^B(\underline{x}) - \eta^A(\underline{x})] \hat{E}_k^A(\underline{x}) \hat{E}_k^B(\underline{x}) \mathrm{dV} \ , \tag{25}$$

Table 1. Description of the two states A and B for the spatial domain $\mathbb{D}$.

state A	state B
$\{\hat{E}_p^A, \hat{H}_q^A\} = \{\hat{E}_p^{inc}, \hat{H}_q^{inc}\}(\underline{x}, s)$	$\{\hat{E}_p^B, \hat{H}_q^B\} = \{\hat{E}_p^{tot}, \hat{H}_q^{tot}\} = \{\hat{E}_p^{\text{inc}} + \hat{E}_p^{\text{sct}}, \hat{H}_q^{\text{inc}} + \hat{H}_q^{\text{sct}}\}(\underline{x}, s)$
$\{\hat{\eta}^A, \hat{\zeta}^A\} = \{\hat{\eta}, \hat{\zeta}\}(\underline{x}, s)$	$\{\hat{\eta}^B, \hat{\zeta}^B\} = \{(\hat{\eta}, \hat{\zeta}), (\hat{\eta}^{\text{sct}}, \hat{\zeta}^{\text{sct}})\}(\underline{x}, s)\{\underline{x} \in \mathbb{D}\backslash\mathbb{D}^{\text{sct}}, \underline{x} \in \mathbb{D}^{\text{sct}}\}$
$\{\hat{J}_p^A, \hat{K}_q^A\} = \{0, 0\}(\underline{x}, s)$	$\{\hat{J}_p^B, \hat{K}_q^B\} = \{0, 0\}(\underline{x}, s)$

where $\delta\hat{Z}_{\alpha\beta}$ is the change of impedance between two states,

$$\delta\hat{Z}_{\alpha\beta} = \hat{Z}_{\alpha\beta}^A - \hat{Z}_{\alpha\beta}^B \ . \tag{26}$$

The electric field strength is linearly dependent on the electric line current density $\hat{I}_\alpha$, so

$$\hat{E}_k^{A,B}(\underline{x}) = \hat{e}_{\alpha;k}^{A,B}(\underline{x})\hat{I}_\alpha^{A,B} \ , \tag{27}$$

where $\hat{e}_{\alpha;k}^{A,B}(\underline{x})$ denotes the electric field strength caused by an electric unit current density. Applying this to equation (25), in combination with the state descriptions, an equation is obtained describing the change of impedance, $\delta\hat{Z}_{\alpha\beta}$, due to an anomaly $\delta\hat{\eta}(\underline{x}) = \hat{\eta}(\underline{x}) - \hat{\eta}^{\text{sct}}(\underline{x})$ in the background medium as

$$\delta\hat{Z}_{\alpha\beta} = \int_{x_i \in \mathbb{D}} \delta\hat{\eta}(\underline{x})\, \hat{e}_{\alpha;k}^{\text{inc}}(\underline{x})\, \hat{e}_{\beta;k}^{\text{tot}}(\underline{x})\text{dV} \ . \tag{28}$$

This representation for the change of the antenna impedance is the basis for the imaging algorithms to be discussed in the next sections.

4. LINEAR INVERSION BASED ON THE BORN APPROXIMATION

We consider a bistatic setup, one transmitter and one receiver, which is described as a two port system ($N = 2$). This can be achieved since only the sum of the product, electric current density times voltage at each port, over all four ports is of interest. It is known that the electric current density at each port of one dipole has the same amplitude but different orientation. So taking the potential difference between the ports of a dipole and multiplying it with the electric current density of one of the end ports, the sum over both dipoles remains the same. Since now the system can be described as if it is a two port system, the impedance matrix in equation (24) becomes a two times two matrix.

The impedance matrix is obtained by measuring for each dipole the electric current density through one port and the potential difference over the two end ports. All the measurements take place at discrete positions of the antenna system. For this reason the position vector $\underline{b}^{(k)} \in \mathbb{D}$ is introduced; this vector points to the middle of both antennas, see figure 5, with the transmitter antenna positioned at $\underline{x} = \underline{x}^t$ and an identical receiver antenna at $\underline{x} = \underline{x}^r$. The distance between the transmitting and the receiving antenna is denoted by the vectorial quantity $\underline{d}$. Measurements are done at discrete frequencies, all elements of the angular frequency domain Ω. We start with the mutual impedance change, equation (28) for $\alpha = 1$ and $\beta = 2$,

$$\delta Z = \delta Z_{1,2}(\underline{b}^{(k)}, \omega) = \int_{\underline{x} \in \mathbb{R}^3} \delta\eta(\underline{x}, \omega)\, \hat{e}_{1,j}^{inc}(\underline{b}^{(k)}, \underline{x}, \omega)\, \hat{e}_{2,j}^{inc}(\underline{b}^{(k)}, \underline{x}, \omega)\text{dV} \ , \tag{29}$$

where $\hat{e}_{1,j}$ and $\hat{e}_{2,j}$ are the electric fields caused by unit currents in the transmitter ($\alpha = 2$) and receiver ($\alpha = 1$). We define a sensitivity function $S(\underline{x}|\underline{b}^{(k)}, \omega)$ as

$$S(\underline{x}|\underline{b}^{(k)}, \omega) = -\hat{e}_j(\underline{x} - \underline{b}^{(k)} - \frac{1}{2}\underline{d}, \omega)\, \hat{e}_j(\underline{x} - \underline{b}^{(k)} + \frac{1}{2}\underline{d}, \omega) \ , \tag{30}$$

where $\hat{e}_j$ is caused by an unit electric line current in one dipole with a reflector, positioned in the origin. Therefore equation (29) changes into

$$\delta Z(\underline{b}^{(k)}, \omega) = \int_{\underline{x} \in \mathbb{R}^3} \delta\eta(\underline{x}, \omega)\, S(\underline{x}|\underline{b}^{(k)}, \omega)\text{dV} \ . \tag{31}$$

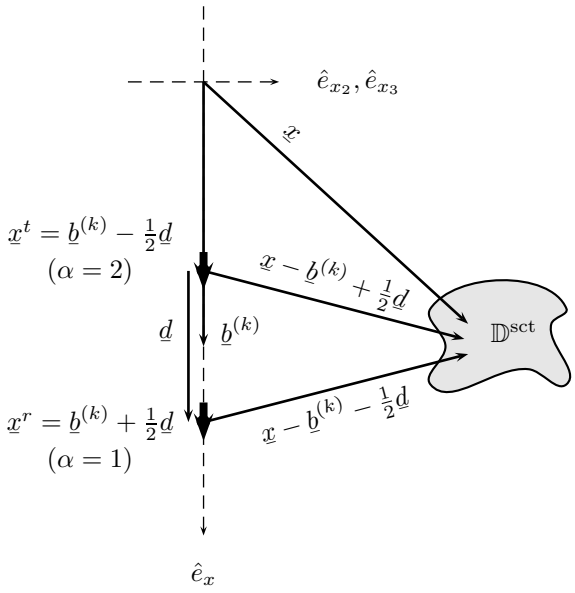

Figure 5. The setup in bistatic mode.

We now rotate both transmitter and receiver in the ϕ direction and move both antennas in the x–direction so that the position of the antenna system in the cylindrical coordinate system becomes $\underline{b}^{(k)} = (x^{(k)}, 0, \phi^{(k)})$. Therefore equation (31) is written in a more explicit way as

$$\delta Z(x^{(k)}, \phi^{(k)}, \omega) = \int_{x=-\infty}^{\infty} \int_{r=0}^{\infty} \int_{\phi=0}^{2\pi} \delta\eta(x, r, \phi, \omega)\, S(x - x^{(k)}, r, \phi - \phi^{(k)}, \omega) dx r dr d\phi \ . \tag{32}$$

In view of the angular convolution and periodicity, the discrete Fourier series of a scalar function $f(\phi)$ is introduced. This series is defined as

$$f(\phi) = \sum_{n=-\infty}^{\infty} f^{(n)} e^{in\phi} \ , \tag{33}$$

where

$$f^{(n)} = \frac{1}{2\pi} \int_{\phi=0}^{2\pi} f(\phi) e^{-in\phi} d\phi \ . \tag{34}$$

Applying the discrete Fourier transforms of equations (33) and (34) to equation (31) leads to decoupled equations in the discrete angular Fourier domain

$$\delta Z^{(n)}(x^{(k)}, \omega) = \int_{x=-\infty}^{\infty} \int_{r=0}^{\infty} \delta\eta^{(n)}(x, r, \omega)\, S^{(n)}(x - x^{(k)}, r, \omega) dx r dr \qquad \text{for } n = -\infty, \ldots, \infty \ , \tag{35}$$

where

$$S^{(n)}(x, r, \omega) = \frac{1}{2\pi} \int_{\phi=0}^{2\pi} e^{-in\phi} S(x, r, \phi, \omega) d\phi \tag{36}$$

$$\delta Z^{(n)}(x^{(k)}, \omega) = \frac{1}{2\pi} \int_{\phi=0}^{2\pi} e^{-in\phi} \delta Z(x^{(k)}, \phi, \omega) d\phi \ . \tag{37}$$

Replacing the latter integrals by finite summations using a trapezoidal integration rule, we arrive at

$$S^{(n)}(x,r,\omega) = \frac{1}{2\pi}\sum_{m=0}^{M} e^{-inm\Delta\phi^{(k)}} S(x,r,m\Delta\phi^{(k)},\omega)\Delta\phi^{(k)} \ , \tag{38}$$

$$\delta Z^{(n)}(x^{(k)},\omega) = \frac{1}{2\pi}\sum_{m=0}^{M} e^{-inm\Delta\phi^{(k)}} \delta Z(x^{(k)},m\Delta\phi^{(k)},\omega)\Delta\phi^{(k)} \ , \tag{39}$$

with $M\Delta\phi^{(k)} = 2\pi$. After obtaining an estimate for $\delta\eta^{(n)}(x,r,\omega)$ for $-N \le n \le N$, the anomaly $\delta\eta(x,r,\phi,\omega)$ in the spatial domain is arrived at

$$\delta\eta(x,r,\phi,\omega) = \sum_{n=-N}^{N} \delta\eta^{(n)}(x,r,\omega)e^{in\phi} \ . \tag{40}$$

4.1. Imaging Based on Back Propagation

In order to obtain an estimate for $\delta\eta(\underline{x})$ we define an error criterion $ERR^{(n)}$

$$ERR^{(n)} = \sum_{x^{(k)}\in\mathbb{D}}\sum_{\omega\in\Omega}\left\| \delta\hat{Z}^{(n)}(x^{(k)},\omega) - \int_{x=-\infty}^{\infty}\int_{r=0}^{\infty} \delta\eta^{(n)}(x,r)\hat{\mathcal{S}}^{(n)}((x,r)|(x^{(k)},r),\omega)dxr\mathrm{d}r \right\|^2 \Delta x^{(k)}\Delta\omega \ . \tag{41}$$

Note that we have taken for computational reasons a new sensitivity function $\mathcal{S}^{(n)}((x,r)|(x^{(k)},r),\omega)$ which is defined by

$$\mathcal{S}((x,r,\phi)|(x^{(k)},r,\phi),\omega) = -\hat{e}_j(\underline{x} - \underline{b}^{(k)} - \frac{1}{2}\underline{d},\omega)\,\hat{e}_j(\underline{x} - \underline{b}^{(k)} + \frac{1}{2}\underline{d},\omega)\,\tilde{S}((x=0,r,\phi)|(0,0,0),\omega = 2\pi f_0) \ , \tag{42}$$

where $\hat{e}_j$ is cylindrical symmetrical wavefield of an electric dipole and $\tilde{S}$ the radiation pattern of the antenna system for fixed frequency $f_0 = 100$ MHz and averaged over a the radial distance. By taking

$$\delta\eta^{(n)}(x,r) = \alpha^{(n)}\Delta\eta^{(n)}(x,r) \ , \tag{43}$$

where $\Delta\eta^{(n)}(x,r)$ is direction and $\alpha^{(n)}$ is a weighting parameter, our error criterion is minimized when

$$\alpha^{(n)} = \frac{\Re\left[\sum_{x^{(k)}\in\mathbb{D}}\sum_{\omega\in\Omega}\delta\hat{Z}^{(n)}(x^{(k)},\omega)\left(\int_{x=-\infty}^{\infty}\int_{r=0}^{\infty}\Delta\eta^{(n)}(x,r)\hat{\mathcal{S}}^{(n)}((x,r)|(x^{(k)},r),\omega)dxrdr\right)^*\right]}{\sum_{x^{(k)}\in\mathbb{D}}\sum_{\omega\in\Omega}\left\|\int_{x=-\infty}^{\infty}\int_{r=0}^{\infty}\Delta\eta^{(n)}(x,r)\hat{\mathcal{S}}^{(n)}((x,r)|(x^{(k)},r),\omega)dxrdr\right\|^2} \ . \tag{44}$$

The numerator

$$\int_{x=-\infty}^{\infty}\int_{r=0}^{\infty}\left(\Delta\eta^{(n)}(x,r)\right)^*\left(\sum_{x^{(k)}\in\mathbb{D}}\sum_{\omega\in\Omega}\left(\hat{\mathcal{S}}^{(n)}(x-x^{(k)},r,\omega)\right)^*\delta\hat{Z}^{(n)}(x^{(k)},\omega)\right)dxrdr \ , \tag{45}$$

attains its maximum if

$$\Delta\eta^{(n)}(x,r) = \sum_{x^{(k)}\in\mathbb{D}}\sum_{\omega\in\Omega}\left(\hat{\mathcal{S}}^{(n)}(x-x^{(k)},r,\omega)\right)^*\delta\hat{Z}^{(n)}(x^{(k)},\omega) \ . \tag{46}$$

Then, $\alpha^{(n)}$ equals

$$\alpha^{(n)} = \frac{\int_{x=-\infty}^{\infty}\int_{r=0}^{\infty}\left\|\Delta\eta^{(n)}(x,r)\right\|^2 dxrdr}{\sum_{x^{(k)}\in\mathbb{D}}\sum_{\omega\in\Omega}\left\|\int_{x=-\infty}^{\infty}\int_{r=0}^{\infty}\Delta\eta^{(n)}(x,r)\hat{\mathcal{S}}^{(n)}(x-x^{(k)},r,\omega)dxrdr\right\|^2} \ . \tag{47}$$

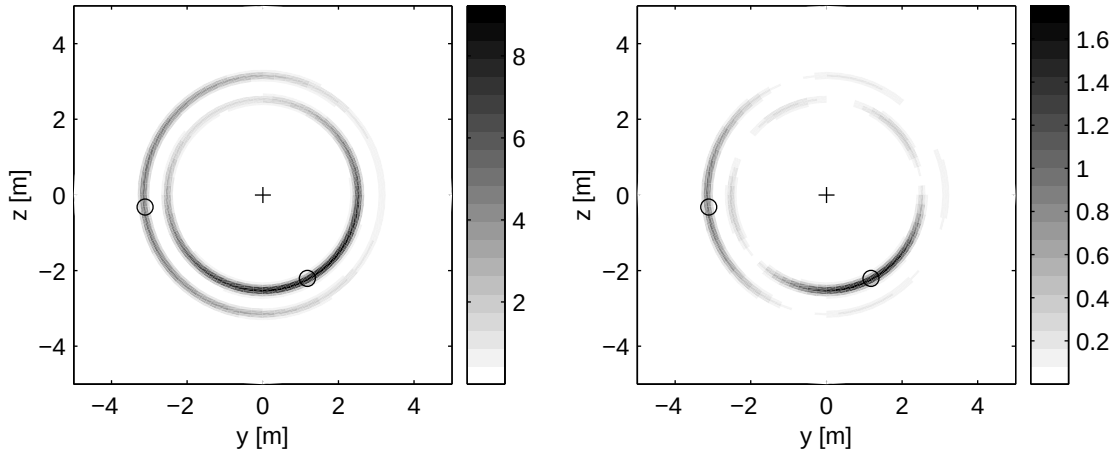

(a) (b)

Figure 6. The result of imaging based on back propagation: $\chi = \Delta\eta$ (a) and minimized back propagation: $\chi = \alpha\Delta\eta$ (b). Circles indicate the position of the objects and the cross indicates the antenna system.

Remark that the special choice for the direction in equation (46) is nothing else than the back propagation of the data to the domain of observation. This is used to obtain a first image, using equation (40). The synthetic data is obtained from equation (32) in combination with (42) where the change of impedance is caused by two point scatterers with medium parameters $\varepsilon_r = 160$, $\mu_r = 1$ and $\sigma = 0$. The data are distorted with 20 % white noise. This result is presented in figure 6(a). The circles indicate the positions of the objects and the cross indicates the position of the antenna system. The image result based on the minimized form of the back propagation is shown in figure 6(b). We observe a significant improvement of the image.

4.2. Imaging via Conjugate Gradient Minimization

In this subsection we use the conjugate gradient method to minimize the error norm of equation (41). In fact, the conjugate gradient method[3] solves for the minimum norm solution of the operator equation

$$f_{k,v}^{(n)} = \sum_{k',l'} L_{k'-k,l'v}^{(n)} \, \eta_{k',l'}^{(n)} \tag{48}$$

in the least-squares sense. In this equation, we have used the following notations

$$f_{k,v}^{(n)} = \delta Z^{(n)}(k\Delta x_1, v\Delta\omega) \ , \tag{49}$$

$$L_{k'-k,l'v}^{(n)} = \mathcal{S}^{(n)}(k'\Delta x' - k\Delta x, l'\Delta r', v\Delta\omega)\Delta x' l' \Delta r' \Delta r' \ , \tag{50}$$

$$\eta_{k',l'}^{(n)} = \delta\eta^{(n)}(k'\Delta x', l'\Delta r') \ . \tag{51}$$

The conjugate gradient scheme computes updates for $\eta_{k',l'}^{(n)}$ After carrying out 100 iterations, the normalized error norm is reduced to $\|ERR^{(n)}\|/\|\delta Z^{(n)}\| = 6.7\,10^{-4}$, see figure 7(a). Subsequently, we compute $\delta\eta(x, r, \phi)$ using equation (40). The result is shown in figure 7(b). Comparison with the results of the minimized back propagation reveals a further improvement in the resolution both in the radial and angular direction.

5. CONCLUSION

In this paper we have shown the design of a new directional borehole radar. Starting with a modeling technique based on the numerical solution of an integral equation for the unknown surface currents on the antenna reflector,

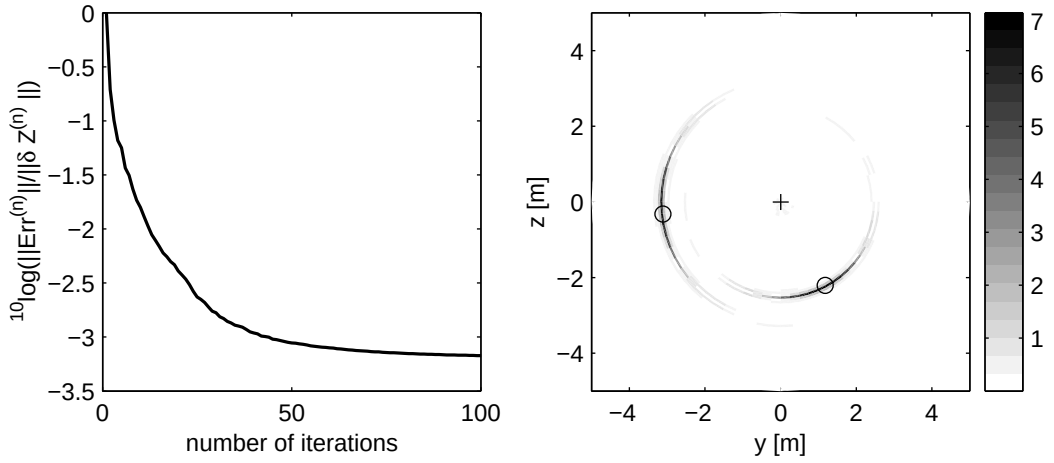

(a) (b)

Figure 7. The results obtained from Conjugate Gradient inversion, (a) the normalized error as a function of the number iterations and (b) the resulting image. Circles indicate the position of the objects and the cross indicates the antenna system.

we have performed many simulations to find the antenna systems that yields the most effective directionality in some specified direction, within the restricted spatial requirements. Good agreement has been observed between the measured radiation pattern of the prototype antenna system and the simulations. Using the modelled radiation patterns one effective dipole radiation pattern is determined and used in the imaging procedures. We have developed an one step imaging algorithm based on minimization of the error in the back propagation results. In fact this step is the first iteration of a conjugate gradient scheme to minimize the error norm between the measured and modelled data. Although this first step yields a good image, it is shown that the resolution can be increased by carrying out more iterations of the conjugate gradient scheme.

ACKNOWLEDGMENTS

During this research support was given by several people. From T&A these include Robert van Ingen, Ronald van Waard, Stefan van der Baan and Michiel van Oers. Further we would like to acknowledge the Netherlands Organisation for Applied Scientific Research, TNO-FEL, the institute that constructed the prototype antenna system. Finally we would like to mention CODEMA, a committee of the Dutch Ministry of Defence, from whom financial support was obtained.

REFERENCES

1. A.P.M. Zwamborn and P.M. van den Berg, "The weak form of the conjugate gradient method for plate problems," IEEE Trans. Antennas Propagat., vol. AP-39, pp. 224-228, 1991.
2. A.T. de Hoop, chapter 28 in *Handbook of Radiation and Scattering of Waves*, Academic Press, London, 1995.
3. R.E. Kleinman and P.M. van den Berg, "Iterative methods for solving integral equations," in *Application of Conjugate Gradient Method to Electromagnetic and Signal Analysis*, PIER 5, Elsevier, New York, 1991.